Electronic Supplementary Material (ESI) for Energy & Environmental Science.

Supporting information

Expanded Hydrated Vanadate for High-Performance Aqueous Zinc-ion Batteries

Chaofeng Liu, Zachary Neale, Jiqi Zheng, Xiaoxiao Jia, Juanjuan Huang, Mengyu Yan, Meng Tian, Mingshan Wang, Jihui Yang*, Guozhong Cao*

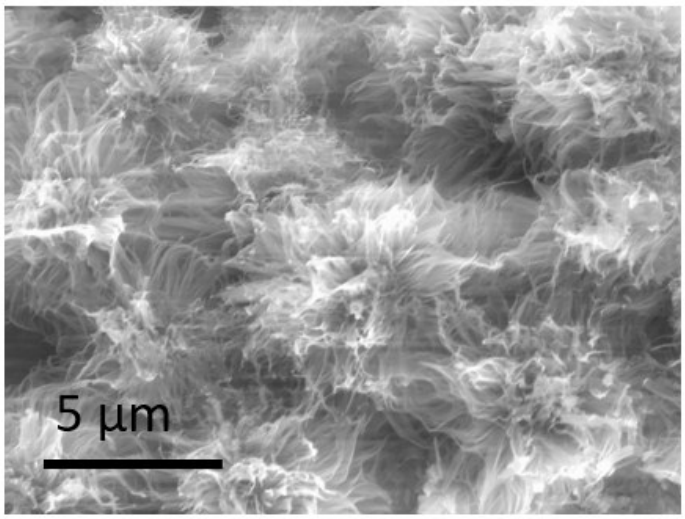

Figure S1. SEM image of MnVO

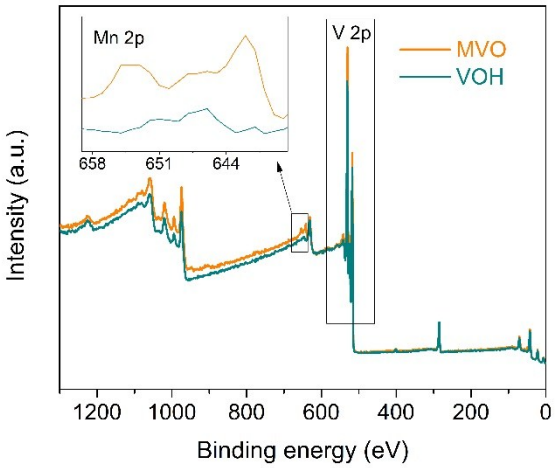

Figure S2. Survey XPS spectra of MnVO and VOH. Mn 2p signal is detected in MnVO but no signal is from S, suggesting no sulfate anion in MnVO as discussed in structure analysis section.

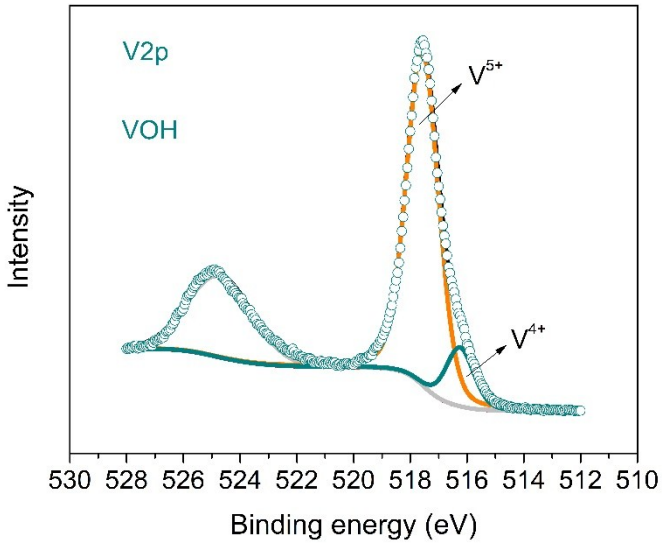

Figure S3. XPS V2p spectrum of VOH. The ratio of V^{4+} is 13.2% calculated by the integrated area.

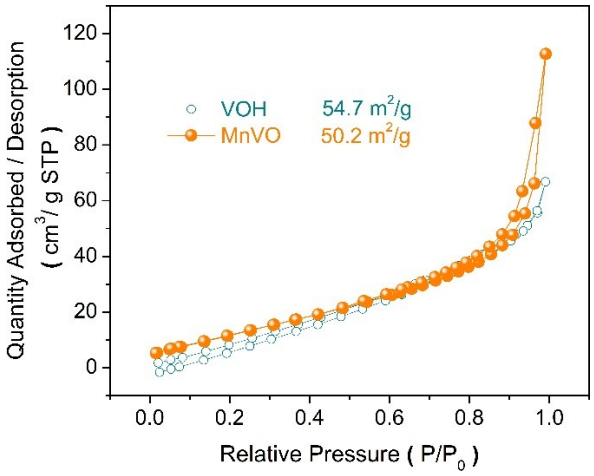

Figure S4. Nitrogen-sorption isotherm of VOH and MnVO. Both samples have a similar BET surface area around 50 m^2/g, so the effects from surface area can be ignored in the comparison of electrochemical performances and the improvements on MnVO can be attributed to the introduction of Mn (II).

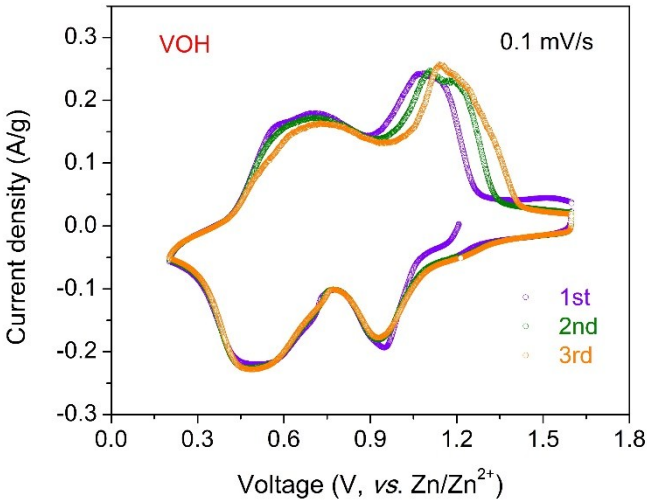

Figure S5. CV curves of VOH collected at 0.1 mV/s with the same working voltage window of 0.2-1.6 V as used in the MnVO test.

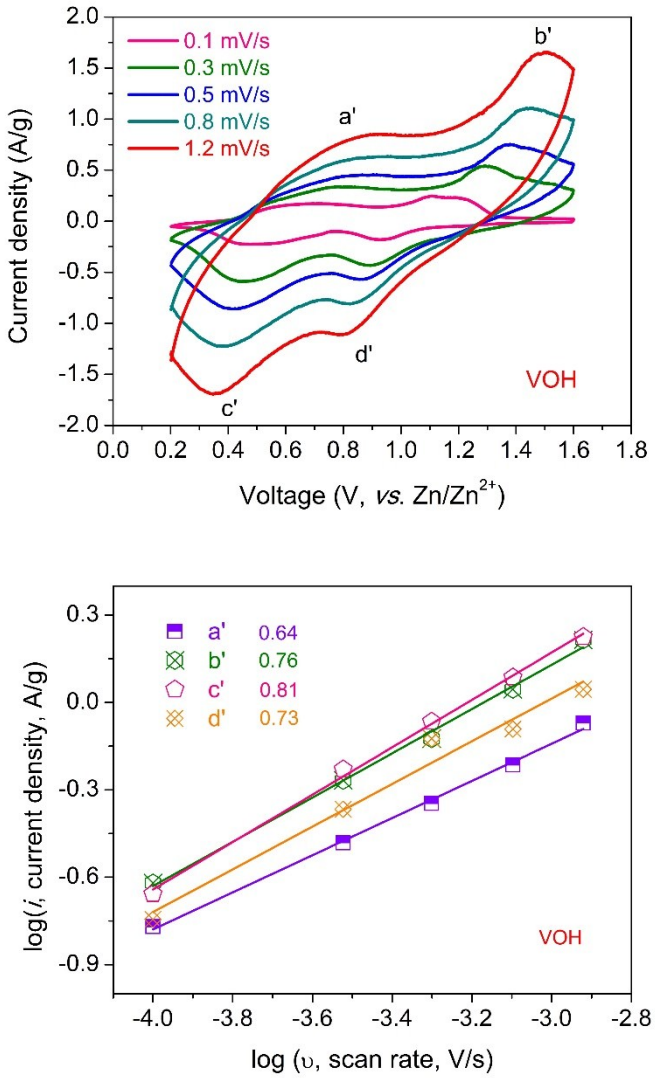

Figure S6. CV curves of VOH and linear relationship between peak currents and sweep rates.

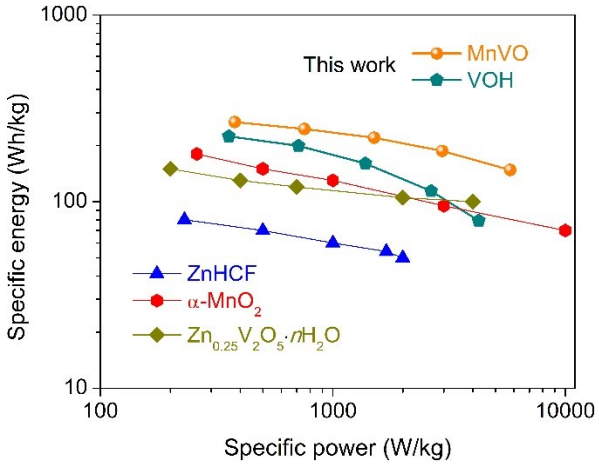

Figure S7. Ragone plot of the Zn-ion batteries with different cathodes, such as ZnHCF,[1] α-MnO_2 [2] and $Zn_{0.25}V_2O_5{\cdot}nH_2O$.[3]

Table S1. Comparison of the cathodes for Zn-ion batteries

Cathode	Voltage window	Specific capacity /Rate performance	Cycling performance	Ref.
MnO_2	1.0-1.8 V	285 mAh/g at 103 mA/g	92% over 5,000 cycles at 1.5 A/g	[3]
V_2O_5	0.4-1.4 V	224 mAh g^{-1} at 100 mA/g	121 mAh g^{-1} maintained over 400 cycles at 1 A/g	[4]
$Na_{0.33}V_2O_5$	0.2-1.6 V	367 mAh/g at 100 mA/g	93% capacity retention over 1,000 cycles at 1 A/g	[5]
$Na_2V_6O_{16}\cdot 1.63H_2O$	0.2-1.6 V	352 mAh/g at 50 mA/g	90% capacity retention over 6,000 cycles at 5 A/g	[6]
$Zn_{0.25}V_2O_5$	0.5-1.4 V	282 mAh/g at 200 mA/g	81% capacity retention after 1,000 cycles at 2.4 A/g	[7]
VO_2(B)	0.3-1.5 V	357 mAh/g at 100 mA/g	91.2% capacity retention after 300 cycles at 0.1 A/g	[8]
CuHCF	0.2-1.2 V	56 mAh/g at 20 mA/g	77% capacity retention after 20 cycles at 0.02 A/g	[9]
ZnHCF	0.8-2.0 V	65 mAh/g at 60 mA/g	76% capacity retention after 100 cycles at 0.3 A/g	[10]
$Mg_xV_2O_5{\cdot}nH_2O$	0.1-1.8 V	353 mAh/g at 50 mA/g	97% capacity retention after 2,000 cycles at 5 A/g	[11]
MnVO	0.2-1.6 V	415 mAh/g at 50 mA/g	96% capacity retention after 2,000 cycles at 4 A/g	This work

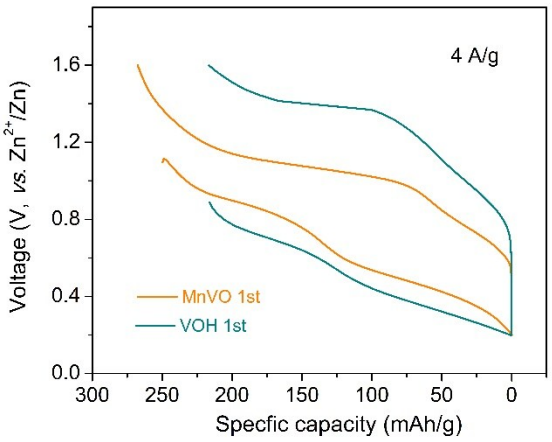

Figure S8. The voltage profile of MnVO tested at a current density of 4 A/g in the 1st cycle. The larger polarization in VOH means a lower energy density.

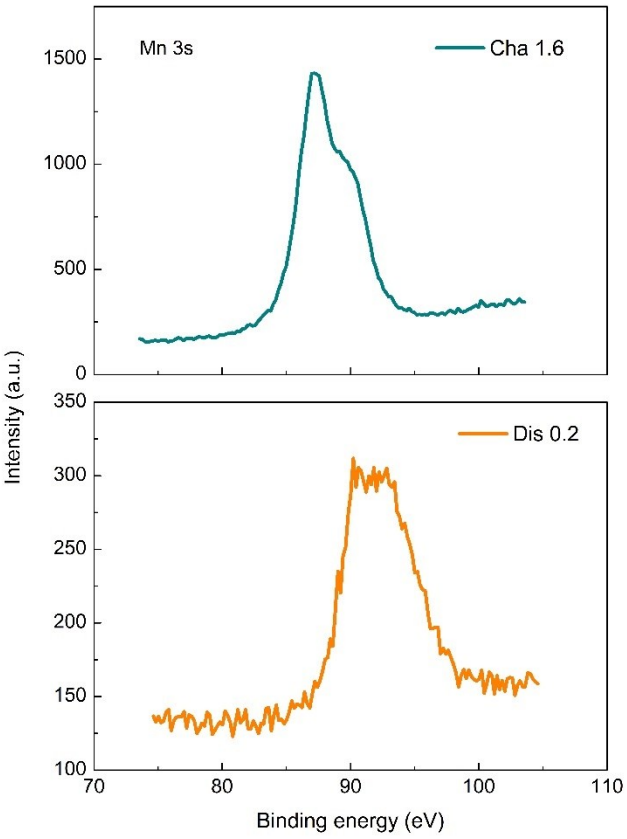

Figure S9. XPS spectra Mn3s at fully charged and discharged states. The detected Mn3s indicates Mn (II) still exist in the crystal lattice, and the difference of binding energy derives from the chemical state of host [VO*n*] polyhedra. In the fully charged state, the binding energy of Mn 3s decreases owing to the strong Coulombic interaction from V^{5+} weakens the attraction from the

nuclei of Mn to the outer electrons and the increase at discharged state attributes to the appearance of more V^{4+} and V^{3+} that lead to a weak interaction from the surrounding ions.

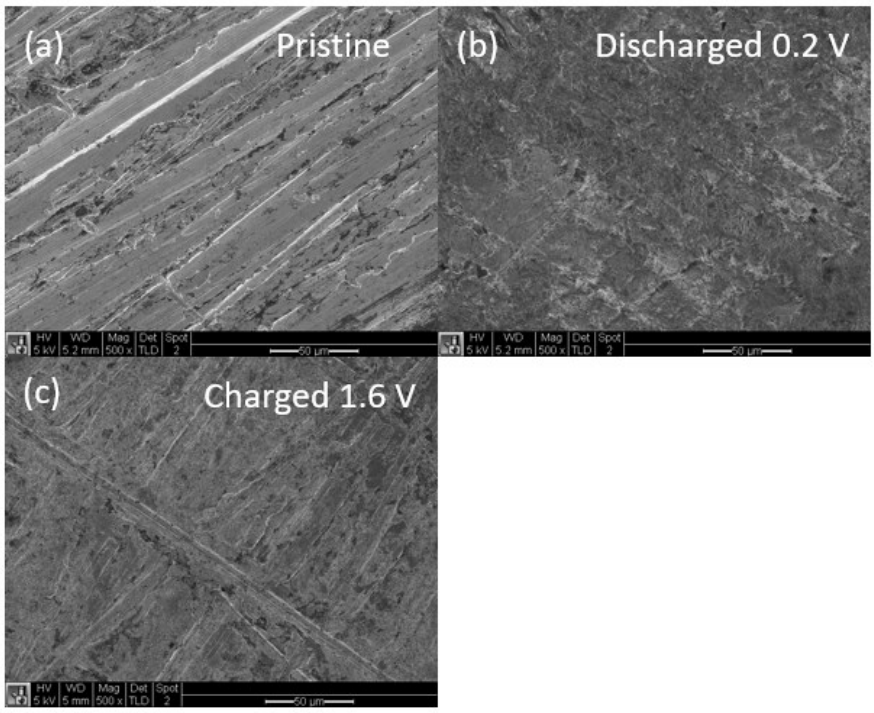

Figure S10. SEM images of Zn anode (a) the pristine, (b) the fully discharged state and (c) the fully charged state.

Zn-ion diffusion coefficients of MnVO and VOH electrodes can be calculated from the low-frequency plots of EIS spectra based on the following equations

$$Z^{'} = R_s + R_f + R_{ct} + \sigma_w \omega^{-0.5} \quad , \qquad (1)$$

$$D_{Li+} = R^2T^2/2A^2n^4F^4C^2\sigma_w^2 \quad , \qquad (2)$$

where ω, A, n, F, C, R, and T stands for the angular frequency, electrode area (0.875 cm^2), reactive electron number per chemical formula (4), Faraday's constant (96, 500 C mol^{-1}), the molar concentration of Zn ions (3.0×10^{-3} mol cm^{-3}), gas constant (8.314 J $mol^{-1}K^{-1}$), and the testing temperature (298 K),

respectively. σw is the linear slopes from the relationship between frequencies and real part of impedance (Figure 6d).

References

1. L. Zhang, L. Chen, X. Zhou and Z. Liu, *Adv. Energy Mater.*, 2015, **5**, 1400930.
2. N. Zhang, F. Cheng, J. Liu, L. Wang, X. Long, X. Liu, F. Li and J. Chen, *Nat. Commun.*, 2017, **8**, 405.
3. H. Pan, Y. Shao, P. Yan, Y. Cheng, K. S. Han, Z. Nie, C. Wang, J. Yang, X. Li, P. Bhattacharya, K. T. Mueller and J. Liu, *Nat. Energy*, 2016, **1**, 16039.
4. J. Zhou, L. Shan, Z. Wu, X. Guo, G. Fang and S. Liang, *Chem. Commun.*, 2018, **54**, 4457-4460.
5. P. He, G. Zhang, X. Liao, M. Yan, X. Xu, Q. An, J. Liu and L. Mai, *Adv. Energy Mater.*, 2018, **8**, 1702463.
6. P. Hu, T. Zhu, X. P. Wang, X. J. Wei, M. Y. Yan, J. T. Li, W. Luo, W. Yang, W. C. Zhang, L. Zhou, Z. Q. Zhou and L. Q. Mai, *Nano Lett.*, 2018, **18**, 1758-1763.
7. D. Kundu, B. D. Adams, V. Duffort, S. H. Vajargah and L. F. Nazar, *Nat. Energy*, 2016, **1**, 16119.
8. J. Ding, Z. Du, L. Gu, B. Li, L. Wang, S. Wang, Y. Gong and S. Yang, *Adv. Mater.*, 2018, **30**, 1800762.
9. Z. J. Jia, B. G. Wang and Y. Wang, *Mater. Chem. Phys.*, 2015, **149**, 601-606.
10. L. Zhang, L. Chen, X. Zhou and Z. Liu, *Adv. Energy Mater.*, 2014, **5**, 1400930.
11. F. Ming, H. Liang, Y. Lei, S. Kandambeth, M. Eddaoudi and H. N. Alshareef, *ACS Energy Lett.*, 2018, **3**, 2602-2609.